COBEM 2021 26th International Congress of Mechanical Engineering
November 22-26, 2021, Virtual Congress, Brazil
ABCM Associação Brasileira de Engenharia e Ciências Mecânicas

COB-2021-1901
THERMODYNAMIC ANALYSIS OF THE HYPERSONIC FLOW OVER A SCRAMJET DEMONSTRATOR CONSIDERING DIFFERENT GAS MODELS

Ramon Carneiro
Aeronautics Institute of Technology, Aerospace Science and Technology Graduate Program, São José dos Campos, Postal Code 12228-900, Brazil.
ramon_cgd@hotmail.com

Angelo Passaro
Institute for Advanced Studies, Department of Aerospace Science and Technology, São José dos Campos, Postal Code 12228-001, Brazil.
angelopassaro@gmail.com

Felipe Pinheiro Maia
Jonatha Wallace da Silva Araújo
Ítalo Sabino Arrais Bezerra
Pedro Paulo Batista de Araújo
Paulo Gilberto de Paula Toro
Federal University of Rio Grande do Norte, Department of Mechanical Engineering, Natal, Postal Code 59072-970, Brazil.
felipepm99@hotmail.com, jonatha_wallace@hotmail.com, italosb94@hotmail.com, araujo.projects@gmail.com, toro11pt@gmail.com

Abstract. *Analytical analysis of hypersonic/supersonic flows is typically conducted assuming the hypothesis of calorically perfect gas. However, the high temperatures reached due to the shock wave compression effects suggest a significant change in the chemical composition of the air, and then, in the thermodynamic properties. In this study, a planar scramjet intake with one single ramp is analyzed assuming three different gas models, calorically perfect gas, frozen gas and chemical and thermodynamic equilibrium gas. The effect of the gas model assumption on the scramjet intake design, and analytical results, i.e., temperature, pressure and density properties are examined. Different operation Mach numbers (7 and 10) conditions are performed considering a flight altitude of 20 km. The results showed that the highest temperature levels downstream (after the oblique shock wave) were obtained in the case of the calorically perfect gas (more conservative case), due to this model not consider endothermic chemical reactions (dissociation and ionization of oxygen and nitrogen, for example). On the other hand, the frozen gas model case results in temperatures lower than that obtained for the calorically perfect gas. This model is a reasonably simple model to implement when compared to the equilibrium air model, for example, and can provide results with better approximation with the reality when compared to the calorically perfect gas. The most representative and realistic results, which consider chemical reactions of the air, are calculated considering air in chemical and thermodynamic equilibrium. This model also predicts lower temperatures because it considers that part of the energy is supplied to the gas particles for dissociation and ionization.*

Keywords: *Calorically perfect gas, Frozen chemistry, Chemical and thermodynamic equilibrium, Oblique shock wave, Hypersonic flow.*

1. INTRODUCTION

One of the main technology for the future of aerospace propulsion is the supersonic combustion ramjet (scramjet). According to Fry (2011), scramjet is a technology that, as one of these main advantages, guarantee high specific impulses for flights with a Mach number greater than 4. The development of scramjet technology involves the study of several areas of knowledge, such as structural mechanics, control systems, aerothermodynamics, and supersonic combustion. From the point of view of aerothermodynamics, a scramjet geometry is designed to ensure that the process of atmospheric air compression, which occurs due to the establishment of oblique shock waves in the intake region, guarantees sufficient conditions for burn fuel in the combustion chamber (Carneiro, 2020). Figure 1 presents an illustrative scheme of a scramjet geometry.

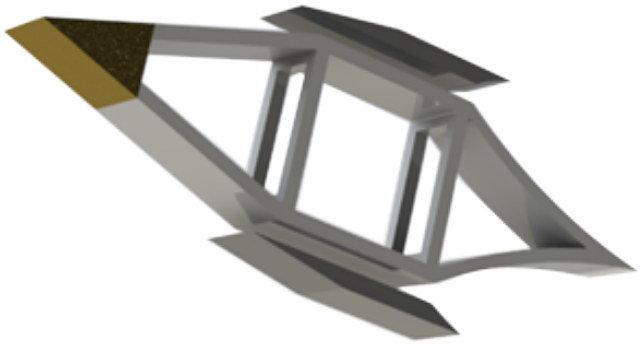

Figure 1. Illustrative scheme of a scramjet geometry.

In the scramjet design process, a factor that significantly impacts the analysis is the air model adopted. Commonly, the calorically perfect gas hypothesis is adopted for air in the most engineering problems. For the scramjet design, most of the papers in literature adopt this simplification, as can be seen in Clark *et al.* (2006), Pajcin *et al.* (2017) and Araújo (2019). However, for high Mach numbers, the hypothesis of air as a calorically perfect gas tends to diverge from the reality for not considering the air dissociation (Anderson, 2006). In these cases, it is known that the air properties change as a function of pressure and temperature.

For designs more coherent with the physics in high speed flows, models that evaluate changes in the air compositions were developed. Among them, can be mentioned the frozen gas model, which corrects the molar mass of the gas as a function of pressure and temperature (Yoder *et al.*, 2008), and the chemical and equilibrium gas model, which considers the absorbed energy by chemical reactions that occur with the dissociated air (Anderson, 2006).

In order to enhance the scramjet design process, the objective of this paper was to evaluate the impact, in terms of dimensional characteristics and the thermodynamic properties, of the use of these three models, e.g., air as an ideal gas, air as frozen gas and air in chemical equilibrium, in the design of a scramjet demonstrator with mixed intake composed by a single 18° compression ramp.

2. METHODOLOGY

2.1 Scramjet intake

In this work, a planar scramjet with a mixed compression system design to perform a fly at an altitude of 20 km (Z) in the dense Earth's atmosphere is analyzed using the three models of gas proposed. Two different Mach number is compared ($M = 7$ and $M = 10$). The intake is designed to be composed by one simple ramp (θ = 18°). Due to the interaction of the hypersonic flow with the compression ramp, it is expected the establishment of a shock wave with a β angle (Figure 2).

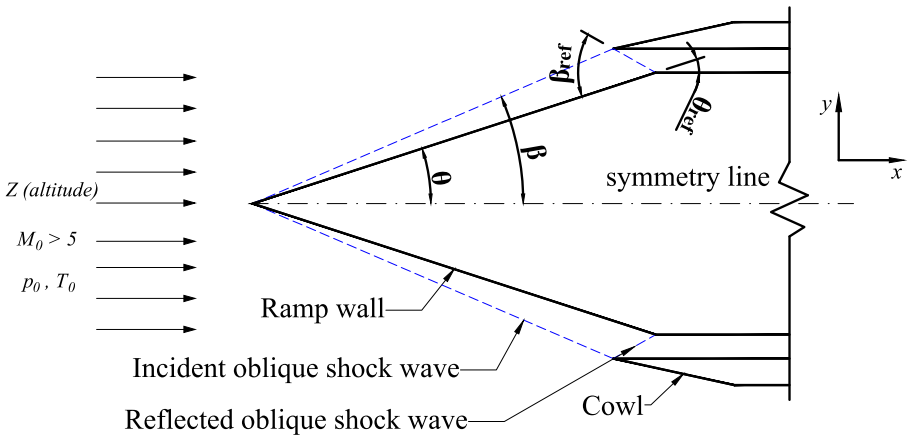

Figure 2. Intake design.

where the *p and T* is the pressure and the temperature, respectively. The index *0* means the freestream condition, and the index *ref* is related to the reflected oblique shock wave.

The thermodynamic properties of the freestream at an altitude of 20 km are computed using the Standard Atmosphere Model (NASA, 1976). The thermodynamic properties, dimensionless quantities and velocities are presented in Table 1 and 2.

Table 1. Thermodynamic atmospheric properties at 20 km altitude. Z and λ are the geometric altitude and mean free path, respectively.

Z	T_0	p_0	ρ_0	λ	a_0	μ_0
km	K	Pa	kg/m^3	m	m/s	N s/m^2
20	216.65	5529.3	0.088910	9.1393×10^{-7}	295.0695	1.4216×10^{-5}

Table 2. Velocities for 20 km of altitude and Mach numbers 7 and 10.

Z	k_n	1° case M_0	1° case V_0	2° case M_0	2° case V_0
km	L = 1 m		m/s		m/s
20	9.1393×10^{-7}	7	2065.3	10	2950.4

where k_n is the Knudsen number, a is the sound speed, μ is the dynamic viscosity, V is the velocity and ρ is the density of the gas.

The most relevant geometric dimensions for the evaluated scramjet intake are presented in Figure 3. Considering a half part of the symmetric intake, H is the height of the intake, R_1 is the length of the compression ramp, L_1 is the length of the compression ramp in the horizontal axis, L_2 is the length of the scramjet isolator, $H_{c.c}$ is the height of the combustion chamber, S_1 and S_2 are the length of the incident oblique shock wave and reflected oblique shock wave, respectively. Positioning the cowl in order to guarantee the shock on-lip and on-corner criteria, the geometric dimensions can be calculated from trigonometric relationships (Equations 1 to 4).

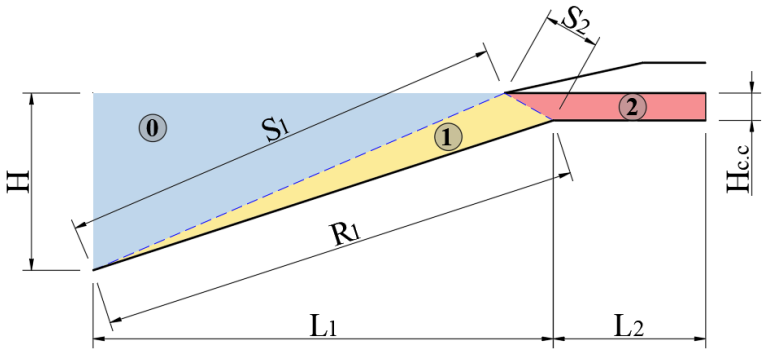

Figure 3. Intake geometric variables and thermodynamic states.

$$S_1 = H/\sin\beta \tag{1}$$

$$R_1 = \frac{H - H_{c.c}}{\sin\theta} \tag{2}$$

$$S_2 = \frac{S_1 \sin(\beta - \theta)}{\sin\beta} \tag{3}$$

$$L_1 = R_1 \cos\theta \tag{4}$$

Three thermodynamic states can be defined in the designed scramjet intake. State 0 corresponds to the freestream at the design altitude (blue color). State 1 corresponds to the airflow downstream the incident oblique shock wave (yellow color), and State 3 corresponds to the airflow downstream the reflected oblique shock wave (red color). In this work, each state are calculated using different gas model. In Figure 4 is presented the scheme of the proposed methodology.

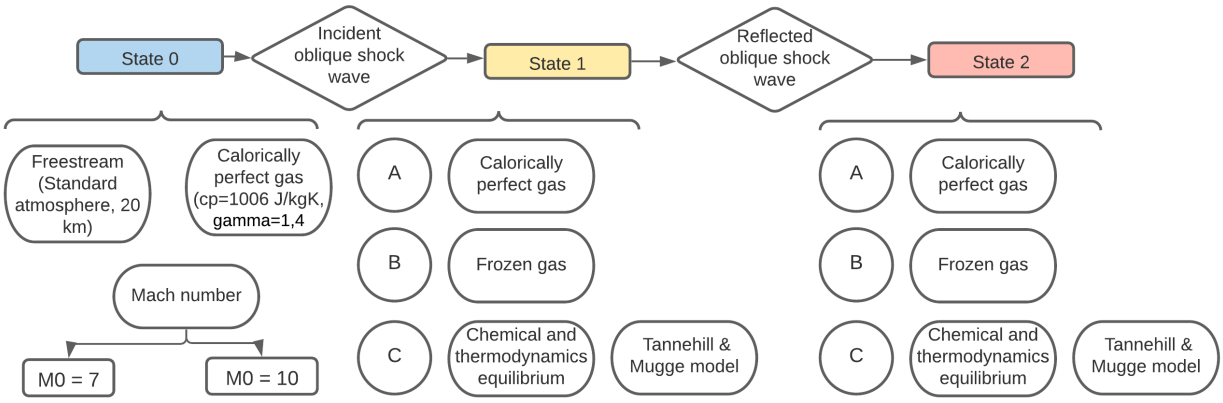

Figure 4. Methodology flowchart.

2.2 Oblique shock wave governing equations

When the flow at supersonic/hypersonic velocity is forced over a wedge with a turn angle (θ), an incident oblique shock wave is established. These waves are extremely thin regions, in the order of mean free path of 10^{-5} cm, and characterize the deflection of current lines due to disturbance generated by the body (Anderson, 1990). By definition, the incident oblique shock wave presents with a relative angle (β) to the upstream flow. The thermodynamic properties and airflow speed are highly influenced by the phenomenon of oblique shock waves, so that the pressure (p), temperature (T) and density (ρ) levels increase, while the Mach number (M) decreases.

When an oblique shock wave hits a solid surface, the reflection of the incident oblique shock wave is established, called the reflected oblique shock wave. In this case, the flow fits the boundary condition that, in most cases involving scramjets, it consists of a flat plate with the purpose of making the current lines parallel to the wall of the combustion chamber.

Considering steady-state and one-dimensional flow, the equations of conservation of mass, momentum and energy applied to an oblique shock wave are given by Anderson (1990).

$$\rho_{in} u_{in,n} = \rho_2 u_{out,n} \tag{5}$$

$$p_{in} + \rho_{in} u_{in,n}^2 = p_{out} + \rho_{out} u_{out,n}^2 \tag{6}$$

$$h_{in} + \frac{u_{in,n}^2}{2} = h_{out} + \frac{u_{out,n}^2}{2} \tag{7}$$

where the index in and out are related to upstream and downstream flow, respectively. u_n is the normal component of the velocity, and h is the enthalpy.

2.3 Calorically perfect gas model

By definition, calorically perfect gas is one in which specific heats (c_p and c_v) can be considered constant, so the ratio between specific heats ($\gamma = c_p/c_v$) is also constant. For these gases, enthalpy and internal energy (e) are only function of the temperature, given respectively by:

$$h = c_p T \tag{8}$$

$$e = c_v T \tag{9}$$

Note that for this model, only the translational and rotational state of energy of the molecules are considered. It is assumed that there are no chemical reactions between the molecules due the increase of temperature or pressure. In this case, the equation of state is valid (Eq. 10).

$$pv = RT \tag{10}$$

From the governing equations (Eq. 5 to 7) and considering the calorically perfect gas hypothesis, the main relationships between Mach number, thermodynamic properties and angles can be obtained in its closed mathematical form for an incident or reflected oblique shock wave (Anderson, 1990), as follow:

$$\tan\theta = 2\cot\beta \left[\frac{\left(M_{in}\sin\beta\right)^2 - 1}{M_{in}^{\ 2}\left(\gamma + \cos 2\beta\right) + 2} \right] \tag{11}$$

$$\frac{p_{out}}{p_{in}} = 1 + \frac{2\gamma}{(\gamma+1)}\left[\left(M_{in}\sin\beta\right)^2 - 1\right] \tag{12}$$

$$\frac{\rho_{out}}{\rho_{in}} = \frac{(\gamma+1)\left(M_{in}\sin\beta\right)^2}{\left[(\gamma-1)\left(M_{in}\sin\beta\right)^2 + 2\right]} \tag{13}$$

$$\frac{T_{out}}{T_{in}} = \frac{p_{out}}{p_{in}}\frac{\rho_{in}}{\rho_{out}} \tag{14}$$

$$M_{out} = \left[\frac{\left(M_{in}\sin\beta\right)^2 + \frac{2}{\gamma-1}}{\frac{2\gamma}{\gamma-1}\left(M_{in}\sin\beta\right)^2 - 1}\right]^{1/2} \frac{1}{\sin(\beta-\theta)} \tag{15}$$

2.4 Frozen gas model

The increase of the airflow temperature due to the oblique shock wave suggests to consider changes in the chemical composition of the flow. A simple way to make this consideration is to estimate the new chemical composition of the flow assuming the equilibrium at defined temperature and pressure calculated after the oblique shock wave. Using this methodology, it is calculated a new specific heat ratio according to the chemical composition of the products and which can be used in Equations (12) to (15). This procedure characterizes the frozen gas model and can be applied when the time for the fluid element to cross a length of the flow field of interest (t_f) is greater than the time for chemical reactions get closer to balance (t_c), thus:

$$t_f >> t_c \tag{16}$$

In this work, the *Gaseq*® software was used to calculate the new composition of the airflow. In Table 3 is presented important assumptions for the evaluated model.

Table 3. Frozen gas model assumptions.

Type of problem	Equilibrium at defined temperature and pressure
Reagents	Air with N_2, O_2 and Ar species
Products	Dissociated air, which may present Ar, N_2, O_2, NO, O, N, N_2O, NO_2 species

Once the composition of the products is estimated by the software, using the Gibbs free energy minimization (Morley, 2005), it is possible to calculate the new mean molecular weight of the air after the shock wave ($M_{w,air}$), the relative constant R, and the value of the specific heat ratio (γ), according to:

$$M_{w,air} = f_1 M_w N_2 + f_2 M_w O_2 + f_3 M_w AR + f_4 M_w NO_2 + f_5 M_w O + f_6 M_w N + f_7 M_w N_2 O + f_8 M_w NO_2 \tag{17}$$

where f_i is the molar fraction of the species.

$$R = R_u / M_{w,ar} \tag{18}$$

and R_u is the universal gas constant, equal to 8.314 $J/(kg - molK)$.

$$\gamma = \frac{c_p}{c_p - R} \tag{19}$$

2.5 Chemical and thermodynamic equilibrium gas model

Considering that the atmospheric air is composed of several chemical species where intermolecular forces are negligible and subject to chemical reactions, the specific heats c_p and c_v are variable and function of temperature, pressure and time.

For the special case of gas in equilibrium, the chemical composition is a function of temperature and pressure ($Ni = f_i(p,T)$, thus, the specific heats $c_p(p,T)$ and $c_v(p,T)$ are function of temperature and pressure too. Note that other state variables can be defined using two properties independent variables. This model is physically the most realistic of the three evaluated in this work. It suits high gas temperature conditions.

In this paper, the method of Tannehil and Mugge is used for the equilibrium gas model. Considering atmospheric airflow, this method inserts the properties of atmospheric air in chemical and thermodynamic equilibrium at high temperature in the calculations of the governing flow equations (Equations 5, 6, 7), by correlations and polynomial fittings between table and calculated data (Tannehill and Mugge, 1974). The enthalpy and temperature are considered function of pressure and density, as follow.

$$h_2 = h(p, \rho) \tag{20}$$

$$T_2 = T(p, \rho) \tag{21}$$

The system of equation to be solved consists of Equations (5, 6, 7, 20, 21), whose unknowns are p_2, h_2, u_2, ρ_2. Also, more two equations are considered for computed the wave angle (β), and the normal component of the income flow (u_1).

The normal component of the free stream velocity is given by:

$$u_1 = V_1 \sin\beta \tag{22}$$

The shock wave angle is calculated using the trigonometric relation:

$$\frac{\tan(\beta - \theta)}{\tan\beta} = \frac{u_2}{u_1} \tag{23}$$

The procedure to calculate the set of equations is based on a iterative method, which first it is solved the Equations (5, 6, 7, 20, 21) (inner loop). Second, it is computed the shock wave angle by Equations (22, 23) (outer loop). The details of the iterative procedure can be found in Moura and Rosa (2013).

3. RESULTS AND DISCUSSIONS

As previously established from the Equations (1) to (4), six scramjet geometries were dimensioned following what is presented in Figure 3, one for each combination of gas model and Mach number. Table 4 presents the set of dimensions obtained for each case.

Table 4. Intake dimensions considering different gas models.

Model	Mach 7						Mach 10					
	S1 [mm]	S_2 [mm]	R_1 [mm]	L_1 [mm]	L_2 [mm]	$H_{c.c}$ [mm]	S_1 [mm]	S_2 [mm]	R_1 [mm]	L_1 [mm]	L_2 [mm]	$Hc.c$ [mm]
Calorically perfect gas	450.3	107.7	539.8	513.4	300	23.18	477.8	94.9	575.9	547.7	300	12.04
Frozen gas	453.1	108.2	543.9	517.3	300	21.92	485.6	93.49	581.3	552.8	300	10.37
Thermodynamic equilibrium gas	468.9	101.8	540.62	514.2	300	22.94	503.1	84.4	579.7	551.3	300	10.87

The dimensions presented in Table 4 are significantly different. The divergence, of at most about 15% for the isolator height, occurs to guarantee the shock-on-lip and shock-on-corner conditions for all geometries. As can be seen in Table 4, the calorically perfect gas model generates the cases with minor ramp length and major isolator height, which indicates lower levels of velocity in the flow inside the isolator.

Following the procedure described above, the thermodynamic properties calculated for the stations 0, 1 e 2 (Figure 3), for Mach number 7 and 10, are summarized in Tables 5, 6 e 7 for calorically perfect gas, frozen gas and chemical equilibrium gas, respectively.

Table 5. Thermodynamic properties calculated using the calorically perfect gas model.

	Calorically perfect gas (Mach 7)			Calorically perfect gas (Mach 10)		
	Station 0	Station 1	Station 2	Station 0	Station 1	Station 2
M	7	3.95	2.68	10	4.60	3.03
θ (deg)		18	18		18	18
β (deg)		24.957	30.43		23.43	28.44
p (kPa)	5.529	55.352	248.777	5.529	101.078	549.607
T (K)	216.65	568.66	959	216.65	868.81	1606.9
u (m/s)	2065.29	1886.29	1665.52	2065.29	2719.34	2431.46

Table 6. Thermodynamic properties calculated using the frozen gas model.

	Frozen (Mach 7)			Frozen (Mach 10)		
	Station 0	Station 1	Station 2	Station 0	Station 1	Station 2
M	7	4.02	2.82	10	4.85	3.35
θ (deg)		18	18		18	18
β (deg)		24.79	29.69		23.035	27.12
p (kPa)	5.529	54.388	239.320	5.529	96.675	524.908
T (K)	216.65	549.45	877.42	216.65	784.94	1335.86
u (m/s)	2065.29	1888.20	1675.05	2065.29	2725.69	2457.06

Table 7. Thermodynamic properties calculated using the chemical and equilibrium gas model.

	Thermodynamic equilibrium (Mach 7)			Thermodynamic equilibrium (Mach 10)		
	Station 0	Station 1	Station 2	Station 0	Station 1	Station 2
M	7	4.08	4.31	10	4.89	3.35
θ (deg)		18	18		18	18
β (deg)		23.9	28.28		22.19	25.82
p (kPa)	5.529	50.940	219.308	5.529	90.193	488.264
T (K)	216.65	539.98	896.69	216.65	782.45	1384.63
u (m/s)	2065.29	1901.7	1707.41	2065.29	2742.6	2498

From the data presented in Tables 5-7, was possible to set up the curves for the fluid temperature and flow velocity variation along a streamline, which are showed in Figures 5 and 6, respectively. The streamline considered starts in freestream, 100 mm from the scramjet leading-edge, and ends in the outlet of the isolator. As can be seen, the position of each station are different for different curves, which is in accordance with Table 4.

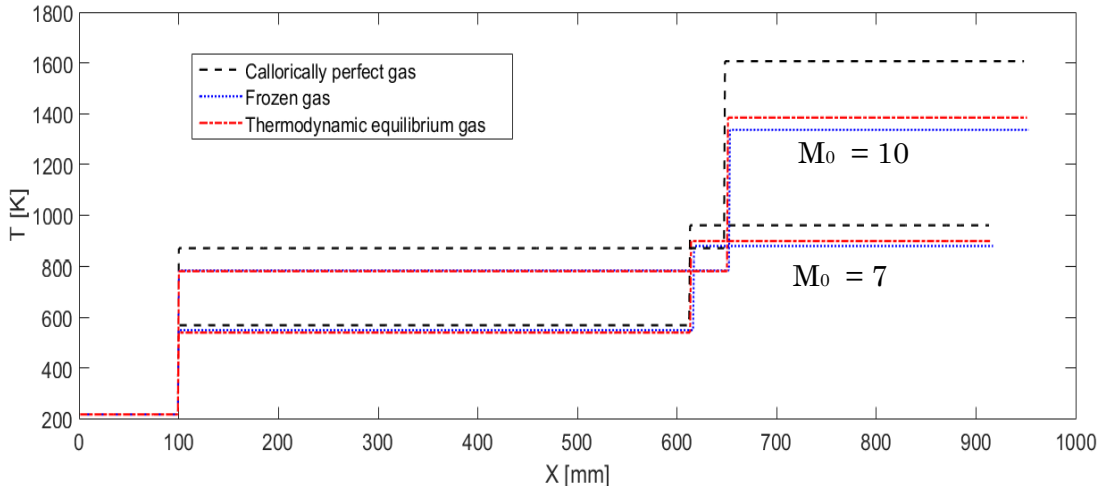

Figure 5. Fluid temperature along a streamline.

The results showed that the highest temperature levels in the isolator (station 3), downstream of the reflected oblique shock wave, were obtained in the case of the calorically perfect gas. This behavior occurs because this model considers only the translational and rotational energy levels for the gas particles, not considering chemical reactions that absorb energy, such as the dissociation and ionization of oxygen and nitrogen. All the energy that would be absorbed by endothermic chemical reactions, in the hypothesis of calorically perfect gas contributes to an increase in the flow temperature.

In addition, the frozen gas and chemical equilibrium gas models resulted in similar levels of temperature in the isolator, with the first one responsible for the lowest values. While the Tannehill and Mugge (1974) model for gas in equilibrium considers the chemical reactions of air and, therefore, the energy supplied to the reagents, the frozen gas model considers the effect of these reactions on the air properties by a correction of the air molar mass, in this case calculated as a function of the flow temperature and pressure. This is a reasonably simple model to be implemented when compared to the equilibrium air model, and it generates similar results, with a better approximation of the reality when compared to the calorically perfect gas model.

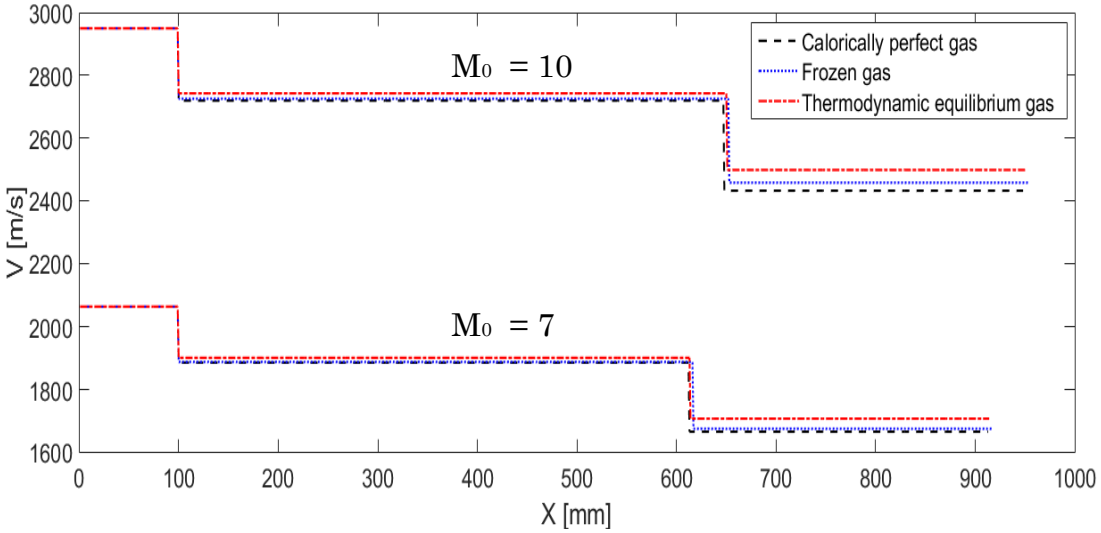

Figure 6. Flow velocity along a streamline.

In a comparison between the Mach number 7 and 10 cases, can be observed that the divergence between the perfect gas model and the other models considered in this paper tends to increase, which is explained by the greater amount of chemical reactions in the case of the Mach number equals to 10, where temperature levels are higher. For example, if this temperature exceeds 2000 K, air dissociation effects arise.

Finally, can be noticed that the β angles calculated for the incident and reflected shock waves are different due the different models adopted for the air properties calculation. Is relevant to note that this difference is the only one responsible for the existence of the different scramjet geometries presented in Table 4.

4. CONCLUSIONS

In this work, a comparative analytical study between three different gas models adopted for the atmospheric air, e.g., calorically perfect gas, frozen gas and chemical equilibrium gas, was developed, in order to enhance the scramjet design process. Considering the results presented in Section 4, following the theory and procedure reviewed in Sections 2 e 3, the following conclusions can be established:

1. The divergence in the isolator height is about 15% between the chemical and thermodynamic equilibrium model and the frozen gas model, considering the operation Mach number equal to 10. This occurs to guarantee the shock-on-lip and shock-on-corner conditions for all geometries, since the shock wave angle β calculated is different for each case.

2. The calorically perfect gas model generates the cases with minor ramp length and major isolator height, which indicates lower levels of velocity in the flow inside the isolator. This model also generates the highest temperature levels in the isolator (station 3).

3. The frozen gas and chemical equilibrium gas models resulted in similar levels of temperature in the isolator. This shows that the frozen gas model is a good choice, since is a reasonably simple model to be implemented when compared to the equilibrium air model, and it generates similar results.

4. The divergence between the perfect gas model and the other models considered in this paper tends to increase with the increase of Mach number. This occurs due to the elevation of the flow temperature levels, and therefore the intensity of endothermic chemical reactions.

5. ACKNOWLEDGEMENTS

This study was financed in part by the Coordenação deAperfeiçoamento de Pessoal de Nível Superior ($CAPES$), Brazil (finance code 001). This work was carried out with the support of the Academic Cooperation Program in National Defense (PROCAD-DEFENSE), grant 88881.387753/2019-01. The authors would like to thanks the Aeronautics Institute of Technology (ITA), the Federal University of Rio Grande do Norte ($UFRN$) and The Institute of Advanced Studies ($IEAv$) for the support given to complete this scientific work. Additionally, the authors appreciate the support provided by the group of Hypersonic Flows ($GEH - UFRN$).

6. REFERENCES

Anderson, J.D., 1990. *Modern Compressible Flow: with historical perspective*. International Edition. McGraw-Hill Education, 2nd edition.

Anderson, J.D., 2006. *Hypersonic and high-temperature gas dynamics*. American Institute of Aeronautics and Astronautics, 2nd edition.

Araújo, J.T.W., 2019. *Análise Numérica do escoamento na seção de captura de ar de um demonstrador scramjet*. Master's degree in mechanical engineering, Universidade Federal do Rio Grande do Norte.

Carneiro, R., 2020. *Estudo Analítico de um Demonstrador da Tecnologia da Combustão Supersônica*. Master's degree in n mechanical engineering, Universidade Federal do Rio Grande do Norte.

Clark, A., Wu, C., Mirmirani, M. and Choi, S., 2006. "Development of an airframe-propulsion integrated generic hypersonic vehicle model". In *44th AIAA Aerospace Sciences Meeting and Exhibit*. American Institute of Aeronautics and Astronautics, Reno, Nevada.

Fry, R., 2011. *The U.S. Navy's Contributions to Airbreathing Missile Propulsion Technology*. doi:10.2514/6.2011-6942.

Morley, C., 2005. "Gaseq, a chemical equilibrium program fow windows". `http://www.gaseq.co.uk/`.

Moura, A.F. and Rosa, M.A.P., 2013. "A computer program for calculating normal and oblique shock waves for airflows in chemical and thermodynamic equilibrium". In *22nd International Congress of Mechanical Engineering (COBEM 2013)*. Associação Brasileira de Engenharia e Ciências Mecânicas, Ribeirão Preto, SP, Brazil.

NASA, 1976. "U.S. Standard Atmosphere". `https://ntrs.nasa.gov/search.jsp?R=19770009539`. Acessed on 2020-03-17.

Pajcin, M.P., Simonovic, A.M., Ivanov, T.D., Komarov, D.M. and Stupar, S.N., 2017. "Numerical analysis of a hypersonic turbulent and laminar flow using a commercial cfd solver". *Thermal Science*, Vol. 21, pp. 795–807.

Tannehill, J.C. and Mugge, P.H., 1974. "Improved curve fits for the thermodynamic properties of equilibrium air suitable for numerical computation using time-dependent or shock-capturing methods, part 1".

Yoder, D.A., Georgiadis, N.J. and O'Gara, M.R., 2008. "Frozen chemistry effects on nozzle performance simulations". In *38th Fluid Dynamics Conference and Exhibit*. American Institute of Aeronautics and Astronautics, Cleveland, Ohio.

7. RESPONSIBILITY NOTICE

The authors are solely responsible for the material included in this scientific article. Additionally, the authors declare that there is no conflict of interest regarding the publication of this scientific article.